

RESTRICTED NONLINEAR BOUNDARY LAYERS OVER A MOVING WALL

Benjamin Minnick

Submarine Maneuvering and Control Division
Naval Surface Warfare Center Carderock Division
9500 MacArthur Blvd., West Bethesda, MD, 20817, USA
benjamin.a.minnick.civ@us.navy.mil

Dennice F. Gayme

Department of Mechanical Engineering
Johns Hopkins University
3400 N. Charles St., Baltimore, MD, 21218, USA
dennice@jhu.edu

ABSTRACT

The restricted nonlinear (RNL) modelling approach is applied to study developing boundary layers over a moving wall. The temporal development of the RNL flow comprises large-scale streamwise-averaged mean dynamics coupled to linearized streamwise varying perturbations supported by a single non-zero streamwise Fourier mode. The evolution of the mean component is shown to share features with spatially developing zero pressure gradient boundary layers, although trends are sensitive to the non-zero streamwise Fourier mode retained in the RNL dynamics. The mode supporting the perturbation is varied to study the effect of including different streamwise-scales on the rate of laminar-to-turbulent transition, skin-friction coefficient predictions, and velocity statistics. The lower wavenumber cases are found to transition to a turbulent state later than higher wavenumber cases. Similar to previous RNL studies of channel flow, lower wavenumber cases predict a smaller skin-friction coefficient and higher streamwise Reynolds stress peak. Interrogation of the RNL components reveals perturbations are active along ramps that develop instantaneously in the streamwise mean. These findings show promise to using the RNL framework to study and interrogate scale interactions within boundary layer flows.

INTRODUCTION

Coherent motions in turbulent boundary layers were studied as early as 1967 by Kline *et al.* (1967), who observed near-wall streaks organize into low- and high-speed regions. Since then, great progress in our understanding of turbulent boundary layers has been gained from interrogating coherent structures and studying their dynamics; see e.g., Jiménez (2018) and references therein. Coherent structures in the form of near-wall streaks have been associated with laminar-to-turbulent transition in boundary layers (Lee & Jiang, 2019). Furthermore, the interaction of these streaks with dominant cross-plane vortical motions is part of the near-wall self-sustaining cycle in wall-bounded turbulence (Hamilton *et al.*, 1995).

Existence of these coherent structures is not limited to the near wall region. Large energy-carrying motions in the outer layer have also been shown to interact in self-sustaining processes (SSPs) in the outer layer (Cossu & Hwang, 2016). The large-scale streaks have also been shown to modulate the amplitude of near-wall streaks (Hutchins & Marusic, 2007). Above the outer-layer, flow in the boundary layer is intermittent and large-scale bulges such as those visualized in Falco (1977) are abundant. These large eddies result in an increased mean streamwise velocity that is well predicted by the law of the wake (Coles, 1956).

The observed importance of coherent structures has motivated a number of reduced order modeling and simulation approaches that simplify the flow based on the dynamical importance of the types of streamwise elongated coherent structures discussed above. For example, the two-dimensional three-velocity component (2D/3C) model restricts the flow to streamwise independent motion but maintains three velocity components. While this representation is capable of redistributing momentum and predicting the subsequent increase in wall-friction associated with wall-bounded turbulence (Orlandi & Jiménez, 1994), the 2D/3C dynamics require persistent forcing to maintain a turbulent state (Gayme *et al.*, 2010). The restricted nonlinear model (RNL) was introduced as a quasi-linear (QL) model that builds on the 2D/3C dynamics through coupling to a streamwise varying perturbation field to achieve self-sustaining turbulent activity (Thomas *et al.*, 2014). In this framework the 2D/3C dynamics serve as the large-scale or mean flow that evolves nonlinearly while the perturbation field is restricted to be linear. Later work demonstrated that accuracy of the RNL framework is improved when the streamwise wave number support of the perturbation field coincides with outer-layer dissipation, see e.g. (Gayme & Minnick, 2019). Similar improvements in accuracy have been shown through augmenting the mean or large scale dynamics (which interact nonlinearly) to include streamwise variation (i.e. defining the mean through a spectral filter, e.g. using a generalized QL (GQL) framework (Kellam, 2019)).

RNL models have been extended to study non-equilibrium flows including spanwise heterogeneous roughness (Minnick *et al.*, 2023). That work specifically focused on the mean component, which was shown to provide insights into large-scale streak-meandering over these surfaces. These extensions demonstrate the versatility of the framework in analyzing a wide range of wall-bounded turbulent flows but thus far studies have been limited to statistically stationary flows. However, a number of engineering flows are best described as spatially or temporally varying boundary layers.

Developing boundary layers have primarily been studied using Reynolds-Averaged Navier-Stokes (RANS) or Large Eddy Simulation (LES) techniques. LES was used by Brandt *et al.* (2004) to study transition in zero pressure gradient boundary layers, while Pozuelo *et al.* (2022) employed LES to study pressure-gradient effects. Zero-pressure gradient boundary layers at arbitrarily high Reynolds numbers have also been studied with the aid of wall-models (Inoue & Pullin, 2011). Temporally developing boundary layers over a moving plate are less studied, but have been shown to be similar to spatially developing boundary layers (Afzal, 1996).

This work employs the RNL modeling technique to study

streamwise structures of a temporally developing boundary layer over a moving plate, thus extending application of the RNL modelling paradigm from statistically stationary flows to developing flows. We investigate the effect of limiting streamwise wave number support of the perturbation dynamics to different small scales by limiting the perturbation field (2) to a series of single non-zero streamwise wavenumbers. In this sense, increasing the non-zero wavenumber reduces the length-scale of small-scale perturbations and the effect of different length scales can be directly interrogated. The results highlight the role of these length scales have on key features of developing boundary layers, such as laminar-to-turbulent transition, skin friction, and shape factor. Such insights will be critical in further developments of QL models for these types of developing flows. We also comment on differences between a boundary layers over a moving plate and zero-pressure gradient boundary layers. Most notably the influence of temporal evolution on the momentum balance as opposed to spatial evolution, thus extending the work of Afzal (1996).

This paper is organized as follows. First the RNL model and the numerical technique are discussed. In the results that follow, skin friction and shape factor predictions for different streamwise wavenumber perturbations is presented. Similarities and differences to spatially developing boundary layers is discussed. Ensemble-averaged velocity statistics are then reported for each RNL simulation at $Re_\rho = 3100$ and compared with statistics from DNS of zero-pressure gradient boundary layers provided by Schlatter & Örlü (2010). The streamwise-varying wavenumber and its effect on transition, boundary layer development, and accurate log-law behavior is discussed throughout. This paper then concludes with a summary of findings and directions for future work.

NUMERICAL TECHNIQUE

We take (x, y, z) to denote the streamwise, wall-normal, and spanwise coordinates respectively; t is used to denote the temporal coordinate. The flow field, $\mathbf{u}_T(x, y, z, t)$, is first partitioned into a streamwise mean component, $\mathbf{U}(y, z, t) = \langle \mathbf{u}_T \rangle_x$, and a perturbation component, $\mathbf{u}(x, y, z, t) = \mathbf{u}_T - \mathbf{U}$. Here the angle brackets with a subscript x denote the streamwise averaging operation. An analogous decomposition is applied to the pressure field p_T .

The RNL model equations are derived by applying this decomposition to the governing equations and then neglecting nonlinear interactions between perturbations that do not contribute to the mean. This leads to the RNL dynamics

$$\partial_t \mathbf{U} + \mathbf{U} \cdot \nabla \mathbf{U} + \rho^{-1} \nabla P - \nu \nabla^2 \mathbf{U} = -\langle \mathbf{u} \cdot \nabla \mathbf{u} \rangle_x, \quad (1)$$

$$\partial_t \mathbf{u} + \mathbf{U} \cdot \nabla \mathbf{u} + \rho^{-1} \nabla p - \nu \nabla^2 \mathbf{u} = -\mathbf{u} \cdot \nabla \mathbf{U}, \quad (2)$$

where ρ is the density, and ν is the kinematic viscosity. Here, continuity requires divergence-free mean and perturbation velocity fields, $\nabla \cdot \mathbf{U} = 0$, $\nabla \cdot \mathbf{u} = 0$. Note, the RNL streamwise mean component (1) remains nonlinear, however the non-linearity in the perturbation component (2) omits the term $\mathbf{u} \cdot \nabla \mathbf{u} - \langle \mathbf{u} \cdot \nabla \mathbf{u} \rangle_x$, which provides order-reduction.

The RNL model equations are solved in a pseudo-spectral solver that employs second-order central finite differencing in the wall-normal, and Fourier transforms in the streamwise and spanwise directions. The terms are treated explicitly using the Adams-Bashforth scheme, except the wall-normal diffusive terms which are treated using the implicit Crank-Nicolson

scheme. The 3/2-rule is used for de-aliasing. The divergence-free condition is enforced by solving the pressure Poisson equation, which, owing to the Fourier transforms, is an ordinary differential equation that is directly inverted.

To simulate a temporally developing boundary layer, the bottom wall is considered stationary and the flow is initialized with a uniform streamwise velocity of $\mathbf{U}(y, z, t = 0) = U$ in (1). The wall-induced shear produces momentum transport upwards, leading to the development of the boundary layer. This is equivalent to taking a reference frame that moves with the bottom wall. The Reynolds number, $Re_t = U^2 t / \nu$, then describes the boundary layer evolution and can be thought of as a surrogate to the Reynolds number $Re_x = Ux / \nu$ for spatially developing boundary layers. To trigger turbulence, random noise is applied to (1) and (2) in the near wall region $y < \delta_0$ for an initial period. Statistics are reported by taking a spanwise average as well as an ensemble average with 400 realizations.

Periodic boundary conditions are applied in the streamwise and spanwise directions. A no-slip boundary condition is used on the bottom-wall and the top boundary condition is taken to be stress-free. The wall-normal and spanwise domain size is $[L_y, L_z] / \delta_0 = [6, 2\pi]$. The domain height is at least 1.5 times higher than the largest 99% boundary layer thickness, δ_{99} . The wall-normal and spanwise grid is considered well-resolved with a grid resolution comparable to DNS. The wall-normal grid is stretched using a hyperbolic tangent function.

Omission of the nonlinearity in the perturbation equation only permits non-zero streamwise Fourier modes that contribute to the mean ($k_x \delta_0 = 0$) to interact. This enables a limited number of streamwise Fourier modes to be simulated. This dynamical restriction is taken advantage of in the numerical approach by simulating in streamwise Fourier space and computing the nonlinear terms of the momentum equation as a convolution, which avoids computationally expensive transforms (Bretheim et al., 2018).

The simplified dynamics also allows the effect of including or neglecting different streamwise length scales on the flow properties to be directly interrogated. To this end we consider several RNL simulations of temporally developing boundary layers over a moving wall in which the perturbation field (2) is limited to a single non-zero streamwise wavenumber over the range $k_x \delta_0 = 1$ to $k_x \delta_0 = 7$.

RESULTS

Figure 1 shows the temporal development of the streamwise mean component for an RNL simulation with $k_x \delta_0 = 4$. Although only one non-zero streamwise mode is active throughout this simulation, the mean component is shown to generate a wealth of cross-plane (yz) scales that evolve in time with Re_t . As momentum is transported upwards, the boundary layer grows in time. Transition to the turbulent state can also be identified near $Re_t \approx 0.22 \times 10^6$, where the instantaneous streamwise mean wall shear stress, $\langle \tau_{xy}^w \rangle_x = \nu \partial_y U|_{y=0}$ is shown to increase rapidly.

Growth of a boundary layer over a moving wall shares similar features to zero pressure gradient boundary layers that develop spatially, however there are differences. Perhaps the most notable difference is the von Kármán integral equation. Upon wall-normal integration of the streamwise momentum equation, the skin-friction coefficient, $c_f = 2(u_\tau / U)^2$ which depends on friction velocity $u_\tau = \sqrt{\tau_w / \rho}$, is equal to the time rate-of-change of the displacement thickness, $c_f \approx (2/U)(d\delta^*/dt)$. Note, we have assumed the motion of the wall is steady and the integrated normal-stress difference is

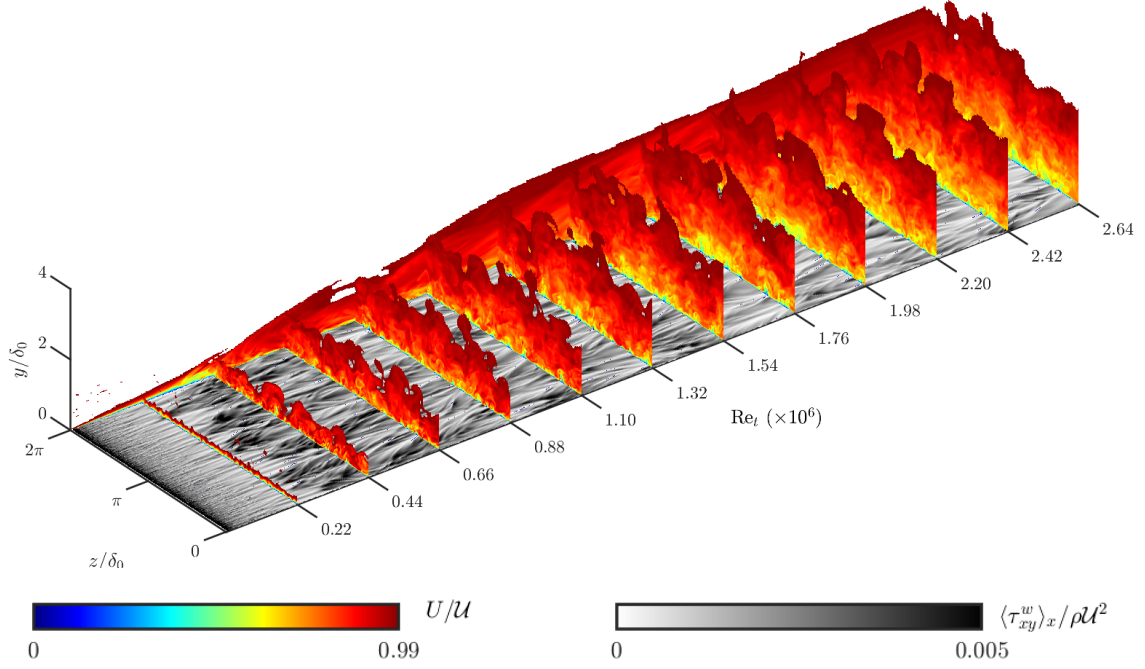


Figure 1. Temporal development of an RNL boundary layer simulation ($k_x \delta_0 = 4$) up to $\text{Re}_t = 2.64 \times 10^6$. Contours of the mean component of the streamwise velocity, U , is shown at various Re_t times and at the $z = 2\pi\delta_0$ plane. Velocity data above $U > 0.99U$ is not shown. Mean streamwise component of the wall shear stress $\langle \tau_{xy}^w \rangle_x$ shown at $y = 0$.

negligible (Schlatter et al., 2008). This is in contrast to the momentum balance for a spatially developing boundary layer, where the skin-friction coefficient is approximately equal to twice the change in the momentum thickness, θ , with respect to x . These thicknesses are respectively defined,

$$\delta^* = \int_0^\infty \left(1 - \frac{\bar{u}_T}{U}\right) dy \quad \text{and} \quad \theta = \int_0^\infty \left(1 - \frac{\bar{u}_T}{U}\right) \frac{\bar{u}_T}{U} dy.$$

This difference in momentum balance between these two types of boundary layers was not noted in Afzal (1996), where instead skin-friction predictions were assumed to follow changes in the momentum thickness. Recognizing that skin-friction for a moving wall depends on the time rate-of-change of the displacement thickness could account for some discrepancy in skin-friction predictions with theory noted in Afzal (1996).

Figure 2 shows skin-friction predictions for all RNL simulations. Included is the time rate-of-change of the displacement thickness as well as the time rate-of-change of the momentum thickness. For all RNL simulations the time rate-of-change of the displacement thickness is shown to coincide well with the skin-friction prediction indicating the von Kármán integral equation involves the displacement thickness, not the momentum thickness.

Another difference between spatially and temporally developing boundary layers is the skin-friction coefficient in the laminar region. If laminar, the governing equations reduce to Stokes first problem where the skin-friction coefficient is $c_f = 2(\pi)^{-1/2} \text{Re}_t^{-1/2} \approx 0.5274 \text{Re}_t^{-1}$, which is higher compared to a Blasius boundary layer, $c_f \approx 0.664 \text{Re}_x^{-1/2}$. For small Re_θ , all RNL simulations are shown to follow the skin-friction coefficient for Stokes flow. After transition, the predictions increase to a higher value. Without a fit to skin-friction

predictions for boundary layers over a moving wall, we compare these turbulent skin-friction coefficient predictions to a fit for spatially developing boundary layers provided by Smits et al. (1983). Despite the differences between the momentum balance of these two boundary layers, the turbulent skin-friction coefficient appears to be similar at large Re_θ .

When comparing skin-friction among the different RNL simulations in figure 2, it is clear the non-zero streamwise

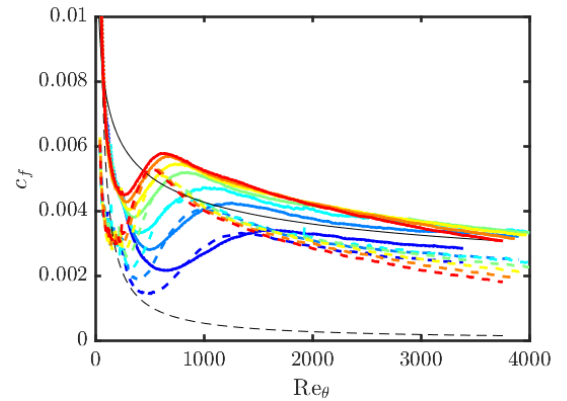


Figure 2. Skin-friction coefficient (thick solid), $(2/U)d\theta/dt$ (thick dashed), and $(2/U)d\delta^*/dt$ (thick dotted, coincides with thick solid lines) for all RNL simulations with streamwise wavenumbers ranging from $k_x \delta_0 = 1$ (blue) to $k_x \delta_0 = 7$ (red). Skin-friction coefficient for a laminar Stokes boundary layer (black dashed) and from the fit, $c_f = 0.024 \text{Re}_\theta^{-1/4}$, from Smits et al. (1983) for a spatially developing turbulent boundary layer (black solid) are included for comparison.

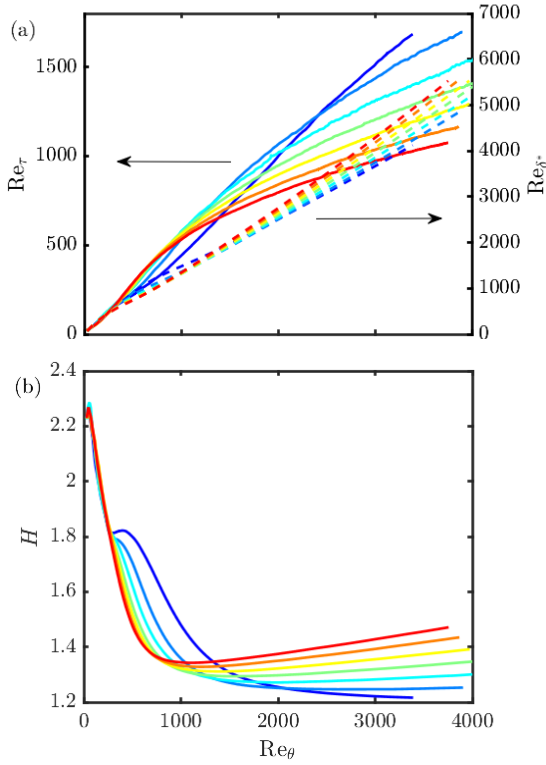


Figure 3. (a) Reynolds numbers Re_τ (solid lines, left vertical axis) and Re_{δ^*} (dashed lines, right vertical axis), as well as (b) shape factor plotted against Re_θ for all RNL simulations with non-zero streamwise modes $k_x \delta_0 = 1$ (blue) to $k_x \delta_0 = 7$ (red).

wavenumber retained in the dynamics influences the development of the boundary layer. Higher wavenumber cases are shown to jump to higher skin-friction values at earlier Re_θ indicating the flow transitions sooner than RNL boundary layers with smaller wavenumbers. Following the continuity equation for the perturbations, $\nabla \cdot \mathbf{u} = 0$, a higher streamwise wavenumber promotes more active cross-plane motions (v, w) therefore leading to earlier transition. In the fully turbulent region at higher Re_θ , the RNL simulations predict similar skin-friction coefficients, although likely approach different asymptotes with increasing Re_θ .

In addition to varying skin-friction, RNL boundary layers with different streamwise wavenumbers are shown to grow differently. Figure 3 shows how various Reynolds numbers and the shape factor, $H = \delta^*/\theta$ vary with Re_θ for all RNL simulations. At small Re_θ , the higher wavenumber cases predict a higher friction Reynolds number, $Re_\tau = u_\tau \delta_{99}/\nu$, which is due to the earlier transition and therefore higher friction velocity. At later Re_θ however, the smaller wavenumber cases achieve a higher Re_τ due to a larger δ_{99} boundary layer thickness. This is not true however for the displacement thickness which is shown to be higher for the higher wavenumber cases suggesting a lower mean velocity profile is predicted at higher Re_θ compared to the smaller wavenumber cases.

There are also notable differences in the shape factor for the different wavenumber cases. Near the transition point the highest wavenumber case shows the displacement thickness relative to the momentum thickness decreases steadily. However for the lowest wavenumber case, there is a sudden increase in displacement thickness compared to the momentum thickness at the transition point. Once a fully developed turbulent state has been reached, the smallest wavenumber

case shows a momentum thickness that grows faster than the displacement thickness. This asymptotic limit changes with increasing wavenumber in a monotonic fashion, where the largest wavenumber case shows a displacement thickness that grows faster than the momentum thickness.

Figure 4 shows ensemble-averaged statistics of each RNL simulation at $Re_\theta = 3100$ compared with DNS data from Schlatter & Örlü (2010). All velocity profiles very near the wall match expected trends, $u^+ \approx y^+$, and show varying behavior in the outer-layer region. We use the ‘+’ superscript to denote scaling by the viscous length-scale, $\delta_\nu = \nu/u_\tau$. Lower wavenumber cases predict a significantly higher intercept compared to higher wavenumber cases. This is similar to previous studies with the RNL model in statistically stationary flows (Gayme & Minnick, 2019). However, for the wavenumbers shown, none of them accurately predict the slope in the outer-layer. It should be noted that the friction Reynolds number range considered here is higher than typically considered within the realm of validity of the RNL model for statistically stationary flows and therefore associated extensions of the model may improve predictions. Furthermore, the wake region for higher wavenumber cases is more prominent, although this may be due to the smaller mean velocity profile in the log-layer. It should also be emphasized that the wake strength for the boundary layer over a moving plate is likely different than a spatially developing boundary layer. Future work will investigate this phenomena further.

In addition to the mean velocity, the Reynolds stress profiles follow similar trends to spatially developing boundary layers. All RNL simulations over-predict the inner-layer peak of the streamwise Reynolds stress, although accuracy im-

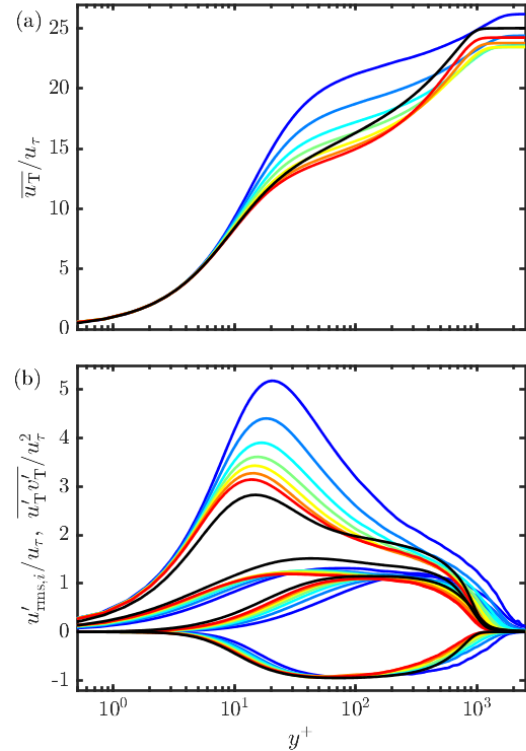


Figure 4. (a) Mean velocity and (b) second-order statistics at $Re_\theta = 3100$ for all RNL simulation with streamwise wavenumbers ranging from $k_x \delta_0 = 1$ (blue) to $k_x \delta_0 = 7$ (red). DNS (black) at $Re_\theta = 3030$ from Schlatter & Örlü (2010) included for comparison.

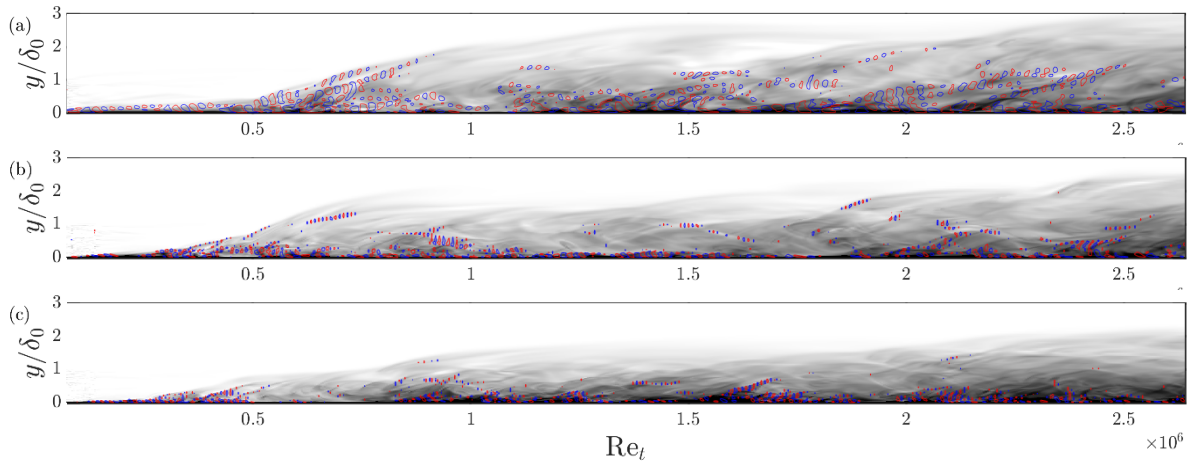


Figure 5. Time history of streamwise velocity at arbitrary spanwise location for RNL simulations with (a) $k_x \delta_0 = 2$, (b) $k_x \delta_0 = 4$, and (c) $k_x \delta_0 = 6$. Streamwise mean component shown as filled contour ranging from $0.5U$ (black) to U (white). Positive and negative fluctuations of the perturbation field contours at $0.1U$ (red) and $-0.1U$ (blue) are superimposed.

proves for higher wavenumber cases. The peak location also changes among wavenumber cases, where lower wavenumber cases predict a peak further from the wall. This shift in peak location occurs for all Reynolds stress components. These findings are consistent with previous studies of the RNL model where the inclusion of smaller more dissipative scales was shown to improve accuracy of moderate Reynolds number RNL simulations (Gayme & Minnick, 2019).

To further understand these RNL predictions for different streamwise wavenumbers, and therefore understand how perturbation wavelength influences boundary layer development, we isolate the mean and perturbation components. Figure 5 shows a time history of these components for RNL simulations with different wavenumbers. For the longer wavelength case shown ($k_x \delta_0 = 2$), a later laminar-to-turbulent transition is shown and a larger boundary layer height is observed in the fully developed turbulent state. This is consistent with the ensemble-average findings shown previously. The mean component is also shown to consist of longer lasting structures for the longer wavelength case. This is the result of the Reynolds-stress like term, $\langle \mathbf{u} \cdot \nabla \mathbf{u} \rangle_x$, in the mean equation.

With only one non-zero Fourier mode simulated, the sign of the perturbation component oscillates for the fixed streamwise position shown. The frequency of this time-fluctuation is proportional to streamwise wavelength. The perturbation component is shown to be advected with the mean, $\mathbf{U} \cdot \nabla \mathbf{u}$, both near the wall and far from the wall. Consistent with the streamwise Reynolds stress, the lower wavenumber case shows a more energetic perturbation component. However all cases show active perturbations in the outer-layer follow along ramp-like structures of the mean component in a manner similar to small-scale organization around large-scale coherent structures studied in Saxton-Fox *et al.* (2022). This suggests the perturbation component is re-energized by the mean shear, $\mathbf{u} \cdot \nabla \mathbf{U}$, which occurs in these regions.

The contribution of the mean and perturbation components to the streamwise Reynolds stress is shown at various points in the boundary layer in figure 6 for these three RNL simulations. Many works have shown the inner-layer peak of these Reynolds stresses does not collapse at different locations within the boundary layer, but instead increases with Reynolds number (see e.g. Yamamoto & Tsuji (2018)). Although over a limited Reynolds number range, this lack of collapse is evident for these RNL simulations. It is interesting to note this behav-

ior does not hold component-wise. The higher wavenumber case shows the mean component inner-layer peak collapses well, and the perturbation component increases. With decreasing wavenumber this is less evident as the peak magnitude of both mean and perturbation component achieve similar values. Furthermore, the outer-layer peak is more pronounced for the higher wavenumber case, although this may be due to the smaller inner-layer peak.

CONCLUSIONS

This work extends the RNL modelling paradigm to study temporally developing boundary layers over a moving wall. These boundary layers share many similarities with spatially developing boundary layers that are more often studied, however there are notable differences. First, the integral momentum equation suggests the skin-friction coefficient is approximately equal to the change of the displacement thickness, not the momentum thickness. Additionally, the Coles' wake parameter is likely different, although this was not confirmed given the varying wake strength predicted by the various RNL simulations. First and second-order statistics in the turbulent region are notably similar to spatially developing boundary layers, particularly when scaled in inner units. This work suggests other streamwise coherent reduced-order models can be used to study boundary layers given simplifications to streamwise or spanwise scale interactions.

A single non-zero streamwise Fourier mode was used in all RNL simulations to represent the perturbation component. This mode varied among simulations to assess its influence on boundary layer development. Consistent with the perturbation continuity equation, RNL simulations with smaller streamwise wavenumbers were shown to transition later than those with higher wavenumbers that promote cross-plane fluctuations. In the turbulent region, a higher mean velocity profile and streamwise Reynolds stress peak was predicted for smaller wavenumber cases, which is comparable to RNL studies on statistically stationary flows. Interrogating mean and perturbation components of the RNL model revealed perturbations are advected with the mean and increase in activity along turbulent ramps due to the mean shear term retained in the perturbation dynamics. Furthermore, higher wavenumber cases showed inner-layer peak collapse of the mean component of the streamwise and spanwise Reynolds stresses; only the perturbation compo-

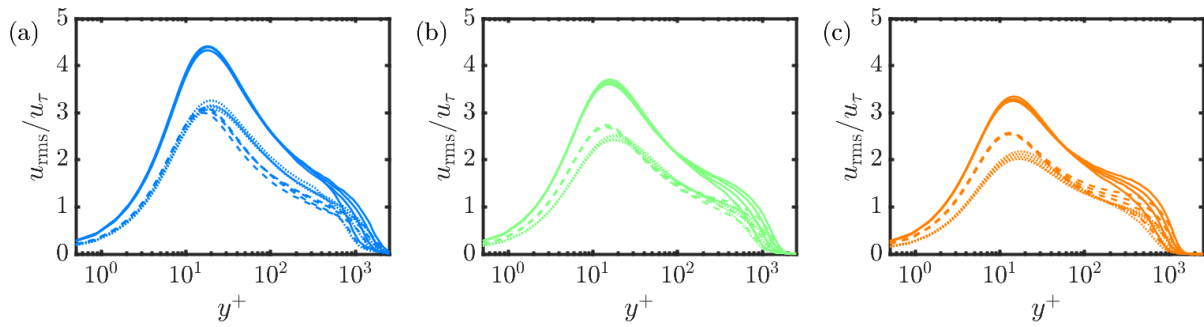


Figure 6. Total (solid) as well as streamwise mean (dashed) and perturbation (dotted) components of the streamwise Reynolds stress at $Re_\theta = 1600, 2350, 3100, 3850$ for (a) $k_x \delta_0 = 2$, (b) $k_x \delta_0 = 4$, and (c) $k_x \delta_0 = 6$.

ment showed amplification with increasing Reynolds number which is more consistent with our intuition of high Reynolds number boundary layers.

There are multiple directions for future work. One is to modify the RNL model parametrization to improve accuracy in first and second-order statistics. RNL studies of channel flow suggest the streamwise wavenumber that most accurately predicts statistics is one that scales with Reynolds number. One could then simulate perturbation dynamics with a streamwise mode that varies in time. Another direction for future work is to accelerate the wall to mimic favorable or adverse pressure gradient effects in spatially developing boundary layers.

ACKNOWLEDGEMENTS

This work was supported by the In-house Laboratory Independent Research (ILIR) program, Problem Element 0601153N, managed by the NSWC Carderock Division Office of Technology and Innovation for the Office of Naval Research. Computations were employed at the Advanced Research Computing at Hopkins (ARCH) core facility (rockfish.jhu.edu), which is supported by the National Science Foundation (NSF) grant number OAC1920103. The authors would also like to thank Mitchell Fowler for the many insightful discussions.

REFERENCES

Afzal, Noor 1996 Turbulent boundary layer on a moving continuous plate. *Fluid Dynamics Research* **17** (4), 181–194.

Brandt, Luca, Schlatter, Philipp & Henningson, Dan S. 2004 Transition in boundary layers subject to free-stream turbulence. *Journal of Fluid Mechanics* **517**, 167–198.

Bretheim, J. U., Meneveau, C. & Gayme, D. F. 2018 A restricted nonlinear large eddy simulation model for high Reynolds number flows. *J. Turbul.* **19**, 141–166.

Coles, Donald 1956 The law of the wake in the turbulent boundary layer. *J. Fluid Mech.* **1** (2), 191–226.

Cossu, C. & Hwang, Y. 2016 Self-sustaining processes at all scales in wall-bounded turbulent shear flows. *Phil. Trans. R. Soc. A* **375**, 20160088.

Falco, R. E. 1977 Coherent motions in the outer region of turbulent boundary layers. *Physics of Fluids* **20**, 124–132.

Gayme, D. F., McKeon, B. J., Papachristodoulou, A., Bamieh, B. & Doyle, J. C. 2010 A streamwise constant model of turbulence in plane Couette flow. *J. Fluid Mech.* **665**, 99–119.

Gayme, D. F. & Minnick, B. A. 2019 Coherent structure-based approach to modeling wall turbulence. *Phys. Rev. Fluids* **4**, 110505.

Hamilton, K., Kim, J. & Waleffe, F. 1995 Regeneration mechanisms of near-wall turbulence structures. *J. Fluid Mech.* **287**, 317–348.

Hutchins, N. & Marusic, I. 2007 Evidence of very long meandering features in the logarithmic region of turbulent boundary layers. *J. Fluid Mech.* **579**, 1–28.

Inoue, M. & Pullin, D. I. 2011 Large-eddy simulation of the zero-pressure-gradient turbulent boundary layer up to $Re_\theta = O(10^{12})$. *J. Fluid Mech.* **686**, 507–533.

Jiménez, J. 2018 Coherent structures in wall-bounded turbulence. *J. Fluid Mech.* **842**, P1.

Kellam, C. B. 2019 Generalized quasilinear simulation of turbulent channel flow. PhD thesis, University of New Hampshire, Manchester, NH, USA.

Kline, S. J., Reynolds, W. C., Schraub, F. A. & Runstadler, P. W. 1967 The structure of turbulent boundary layers. *J. Fluid Mech.* **30** (4), 741–773.

Lee, Cunbiao & Jiang, Xianyang 2019 Flow structures in transitional and turbulent boundary layers. *Phys. Fluids* **31** (11), 111301.

Minnick, Benjamin A., Zhu, Xiaowei & Gayme, Dennice F. 2023 Restricted nonlinear scales of turbulent secondary flows over spanwise heterogeneous roughness. *International Journal of Heat and Fluid Flow* **104**, 109212.

Orlandi, P. & Jiménez, Javier 1994 On the generation of turbulent wall friction. *Phys. Fluids* **6** (2), 634–641.

Pozuelo, Ramón, Li, Qiang, Schlatter, Philipp & Vinuesa, Ricardo 2022 An adverse-pressure-gradient turbulent boundary layer with nearly constant $\beta \simeq 1.4$ up to $re_\theta \simeq 8700$. *J. Fluid Mech.* **939**, A34.

Saxton-Fox, Theresa, Lozano-Durán, Adrián & McKeon, Beverley J. 2022 Amplitude and wall-normal distance variation of small scales in turbulent boundary layers. *Phys. Rev. Fluids* **7**, 014606.

Schlatter, P., Brandt, L., De Lange, H. C. & Henningson, D. S. 2008 On streak breakdown in bypass transition. *Phys. Fluids* **20** (10), 101505.

Schlatter, Philipp & Örlü, Ramis 2010 Assessment of direct numerical simulation data of turbulent boundary layers. *J. Fluid Mech.* **659**, 116 – 126.

Smits, A. J., Matheson, N. & Joubert, P. 1983 Low-reynolds-number turbulent boundary layers in zero and favourable pressure gradients. *Journal of Ship Research* **27**, 147–157.

Thomas, V. L., Lieu, B. K., Jovanović, M. R., Farrell, B. F., Ioannou, P. J. & Gayme, D. F. 2014 Self-sustaining turbulence in a restricted nonlinear model of plane couette flow. *Phys. Fluids* **26** (10), 105112.

Yamamoto, Yoshinobu & Tsuji, Yoshiyuki 2018 Numerical evidence of logarithmic regions in channel flow at $Re_\tau = 8000$. *Phys. Rev. Fluids* **3**, 012602.